Received May 13, 2019, accepted June 8, 2019, date of publication June 24, 2019, date of current version August 15, 2019.

Digital Object Identifier 10.1109/ACCESS.2019.2924463

Dual-Polarized Low-Profile Filtering Patch Antenna Without Extra Circuit

YAOHUI ZHANG[1], YONGHONG ZHANG[1], DAOTONG LI[2,3], (Member, IEEE), ZHONGQIAN NIU[1], AND YONG FAN[1], (Member, IEEE)

[1]School of Electronic Science and Engineering, University of Electronic Science and Technology of China (UESTC), Chengdu 611731, China
[2]Center of Aerocraft TT&C and Communication, Chongqing University, Chongqing 400044, China
[3]State Key Laboratory of Millimeter Waves, Nanjing 210096, China

Corresponding author: Daotong Li (dli@cqu.edu.cn)

This work was supported in part by the National Natural Science Foundation of China under Grant 61801059, in part by the Opening subject of State Key Laboratory of Millimeter Waves under Grant K202016, in part by the Basic Research and Frontier Exploration Special of Chongqing Natural Science Foundation under Grant cstc2019jcyj-msxmX0350, in part by the Chongqing Special Found of Technology R&D for Academician under Grant cstc2018zdcy-yszxX0001.

ABSTRACT This paper proposes a novel dual-polarized filtering patch antenna without an extra circuit. The proposed antenna shows a quasi-elliptic filtering response with four radiation nulls. One radiation null is achieved with a stacked patch, and three more radiation nulls are introduced by the split ring resonators (SRRs) placed inside the antenna aperture. The SRR can achieve one radiation null, and the shorted SRR (SSRR) can achieve two radiation nulls for its odd and even modes. This filtering antenna is fabricated on two stacked substrates with three metallic layers, which is suitable for integration. As demonstrations, two antennas are designed to meet the applications for the 5G band (4.8-5 GHz) for S11 < -10 dB with the total profile of 0.06 λ_L, where λ_L is the free-space wavelength at the lowest operating frequency. The antenna implemented on FR4 substrate achieves an average gain of 5 dBi, while the antenna fabricated on two substrates, Rogers-4350 and FR4, can improve the realized gain to over 6 dBi. The measured isolation is better than 20 dB within the operating band. The out-of-band gain suppression level is more than 15 dB within the 3.4–3.6 GHz and more than 20 dB for WLAN band.

INDEX TERMS Filtering antenna, dual-polarized, low-profile, split ring resonator, stacked patch.

I. INTRODUCTION

With the development of the wireless communication systems, more diverse means of communication systems are established with their own frequency bands. Dual-polarized antennas working in different bands are usually needed to meet the requirements of different systems. However, when other frequency bands are close to the working band, the interference from other bands can become a problematic issue for the working systems. Although increasing the spacing between antenna elements can reduce the interference, the communication equipment would become bulky. Instead, designing the filtering antenna with lower out-of-band radiation can be an effective way to suppress the interference from other bands [1].

Various types of filtering antennas have been proposed in references [2]–[26], including single-polarized antennas [2]–[15], dual-polarized antennas [16]–[24] and circular-polarized antennas [25], [26]. Works in [2]–[9] realize single-polarization and filtering behaviors by cascading filtering circuits and antennas. Nevertheless, extra filtering circuits usually occupy additional area and cause insertion loss. Works in [10]–[13] achieve low out-of-band radiation without extra circuits, and the metasurface antennas [14], [15] are utilized to achieve low profile and high gain with filtering performance. However, these single-polarized antennas are difficult to be extended to dual-polarized ones.

Dual-polarized filtering antennas [16]–[24] have been reported for different applications. The designs in [16]–[23] integrate extra filtering circuits in the antenna feeding networks. As mentioned above, additional volume and insertion loss of filtering circuits are inescapable. A novel dual-polarized filtering antenna without extra filtering circuit is proposed in [24] for the first time by modifying the H-shaped coupling feeding structure. The H-shaped feeding network is designed inside the antenna, so the antenna needs to be designed with two substrates and four metallic layers, making the antenna unsuitable for integration.

The associate editor coordinating the review of this manuscript and approving it for publication was Xiu Yin Zhang.

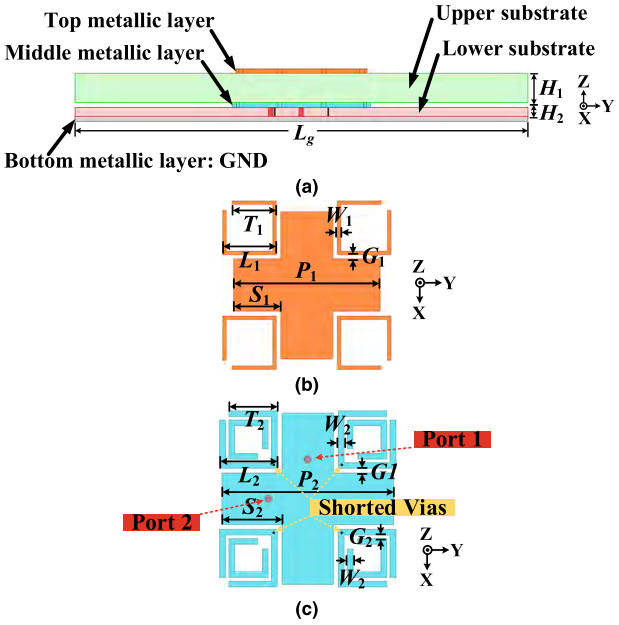

FIGURE 1. The proposed antenna. (a) Side view of the proposed antenna. (b) Top metallic layer. (c) Middle metallic layer. ($L_g = 50$, $H_1 = 3.2$, $H_2 = 1$, $P_1 = 12.7$, $P_2 = 14.9$, $S_1 = 4.1$, $S_2 = 5.2$, $L_1 = 4.6$, $L_2 = 5$, $T_1 = 3.8$, $T_2 = 4.2$, $G_1 = 0.4$, $G_2 = 0.3$, $W_1 = 0.3$ and $W_2 = 0.5$ mm).

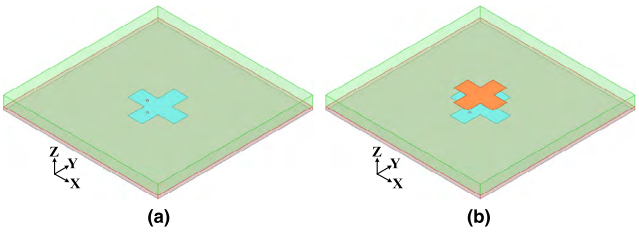

FIGURE 2. (a) Single-patch antenna. (b) Double-patch antenna.

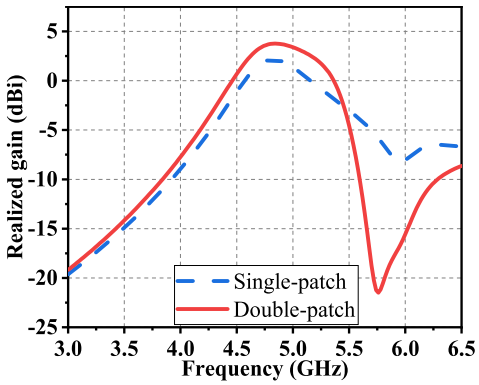

FIGURE 3. Realized gain of the single-patch antenna and the double-patch antenna at the boresight direction.

In this paper, a novel dual-polarized filtering patch antenna without extra circuit is presented. This patch antenna is fed directly by two feeding probes and fabricated on two stacked substrates with three metallic layers, which is suitable for integration. One radiation null is achieved with the stacked patch, one radiation null is produced by the split ring resonators (SRRs) [27], [28], and two more radiation nulls are introduced by the shorted SRRs (SSRRs) [29]–[32] for its odd and even modes. The antenna is designed to meet the applications for the 5G band (4.8-5 GHz) for VSWR < 2 with the total profile of 0.06 λ_L. The antenna implemented on FR4 substrate achieves an average gain of 5 dBi, while the antenna fabricated on two substrates, Rogers-4350 and FR4, can improve the realized gain to over 6 dBi. The measured isolation is better than 20 dB within the operating band. The out-of-band gain suppression level is more than 15 dB within the 3.4-3.6 GHz and more than 20 dB for WLAN band.

II. ANTENNA DESIGN

A. STRUCTURE OF ANTENNA

Fig. 1 displays the configuration of the proposed filtering antenna. As shown in Fig. 1(a), the proposed antenna is fabricated on two stacked FR4 substrates with three metallic layers. These two substrates have the permittivity of $\varepsilon_r = 4.4$ with different thickness. The top metallic layer of the proposed antenna is presented in Fig. 1(b). The top layer includes the stacked patch and four one-turn SRRs. As shown in Fig. 1(c), the middle metallic layer is composed of the driven patch and four SSRRs with shorted vias. The SSRR utilizes two-turn SRR to lower the resonant frequency. The bottom layer of the antenna is the metallic ground. The antenna is fed by two coaxial cables to achieve orthogonal polarization. The evolution of the proposed filtering antenna is explained in the following section. Due to the symmetry of the structure, only the results of port 1 are analyzed.

B. ANALYSIS OF ANTENNA DESIGN

In order to demonstrate the mechanism of two radiation nulls in the upper stop band, the antennas with single and double patches are compared. Fig. 2(a) and (b) are the single-patch antenna and the double-patch antenna, respectively. The realized gain at the boresight direction of these two antennas are presented in Fig. 3. As depicted in Fig. 3, the realized gain within the working band can be improved by using the upper patch as a director, and one radiation null at the boresight direction can be introduced to the higher band of the stacked antenna [10], compared with the single-patch antenna. When the port 1 is driven, the 3-D radiation pattern of the stacked antenna at the radiation null frequency (5.7 GHz) is shown in Fig. 4. There is a radiation null at the broadside direction of the 3-D radiation pattern, resulting in a deep radiation null in Fig. 3. The current distributions on the driven patch and the upper patch at 5.7 GHz (radiation null) are displayed in Fig. 5(a) and (b). It can be seen that the currents on left and right sides of the patch are out-of-phase, as well as the currents on top and bottom sides of the patch. Therefore, the radiation caused by the out-of-phase currents is canceled, producing a radiation null.

Next, four one-turn SRRs are placed inside the stacked antenna aperture in the top metallic layer to introduce a

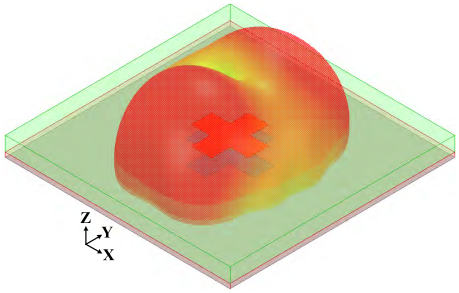

FIGURE 4. 3-D radiation pattern of the stacked antenna at 5.7 GHz.

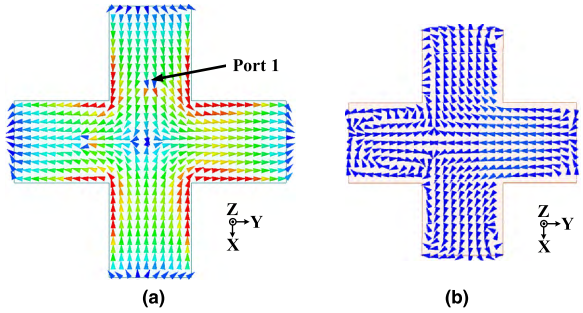

FIGURE 5. Current distributions at 5.7 GHz for the stacked antenna on (a) the driven patch, and (b) the upper patch.

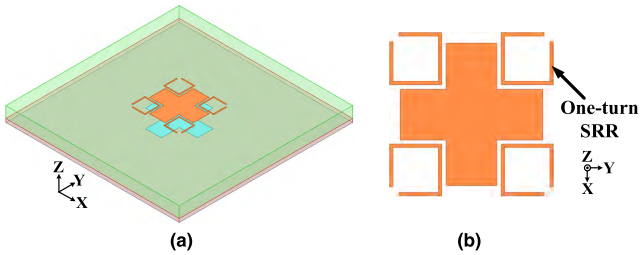

FIGURE 6. The stacked antenna with four one-turn SRRs. (a) Perspective view. (b) Top metallic layer.

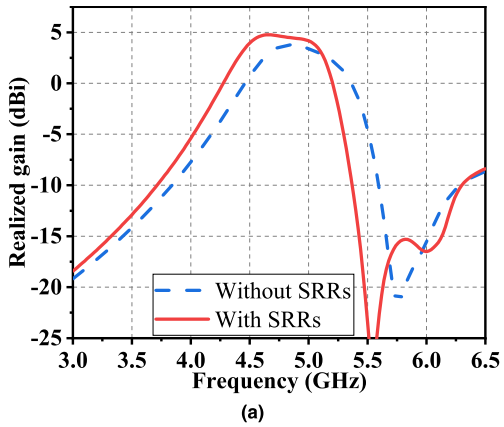

FIGURE 7. Realized gain of the stacked antenna with and without four one-turn SRRs at the boresight direction.

second radiation null, as shown in Fig. 6. The realized gain of the stacked antenna with and without four one-turn SRRs at the boresight direction is displayed in Fig. 7. It can be seen that the upper patch with four one-turn SRRs can introduce one more radiation null (6 GHz) in the higher frequency band, and the first radiation null is moved to 5.5 GHz. The current

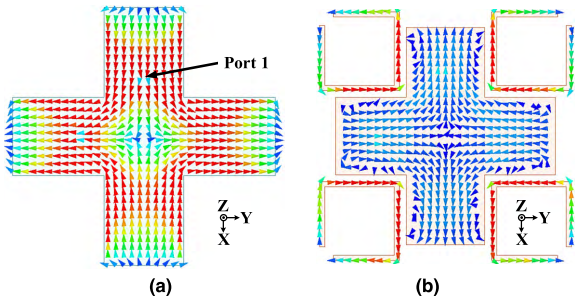

FIGURE 8. Current distributions at 6 GHz for the stacked antenna with four one-turn SRRs on (a) the driven patch, and (b) the top metallic layer.

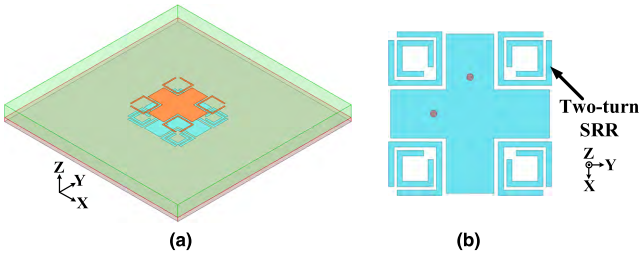

FIGURE 9. The stacked antenna with four two-turn SRRs. (a) Perspective view. (b) Middle metallic layer.

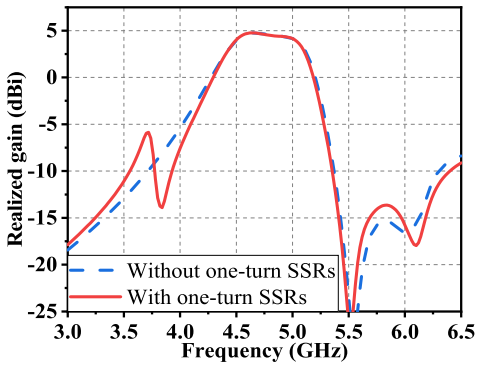

FIGURE 10. Realized gain of the stacked antenna with and without four two-turn SRRs at the boresight direction.

distributions on the driven patch and the top metallic layer at 6 GHz (radiation null) are displayed in Fig. 8(a) and (b). The currents on the driven patch and four SRRs are symmetrical about the X-axis and Y-axis. That is, the currents on left and right sides of the patch are out-of-phase, so is the currents on top and bottom sides, resulting in a radiation null at the boresight direction. At the same time, the energy will be constrained with the oscillation inside the SRRs.

In order to introduce a radiation null to the lower frequency band, the two-turn SRRs (traditional SRR) with compact size are adopted. As shown in Fig. 9, four two-turn SRRs are placed inside the driven patch aperture in the middle metallic layer. The realized gain of the stacked antenna with and without four two-turn SRRs at the boresight direction is displayed in Fig. 10. It can be seen that the two-turn SRRs can introduce one radiation null (3.8 GHz) in the lower stop band, and a quasi-elliptic filtering response is achieved.

Finally, the SSRRs are utilized to produce two radiation nulls in the lower stop band using the odd and even resonant

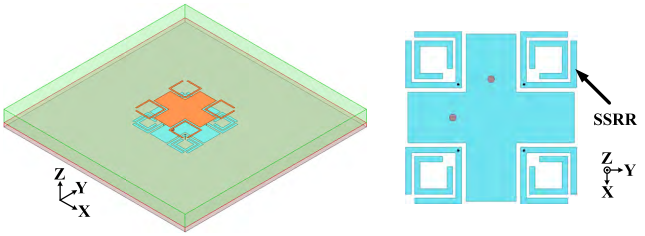

FIGURE 11. The stacked antenna with four SSRRs. (a) Perspective view. (b) Middle metallic layer.

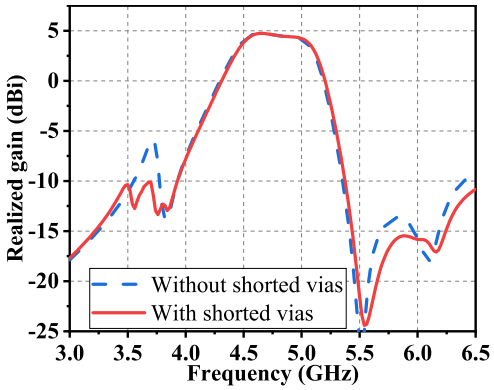

FIGURE 12. Realized gain of the stacked antenna with and without four shorted vias at the boresight direction.

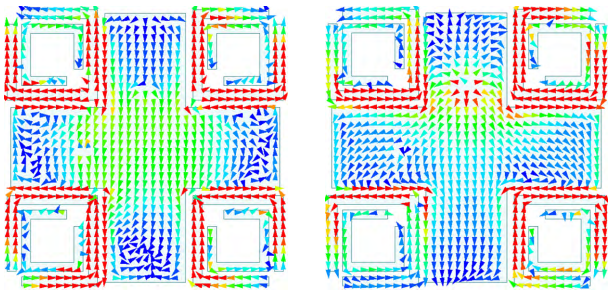

FIGURE 13. Current distributions for the stacked antenna with four SSRRs on the middle metallic layer at (a) 3.55 GHz, and (b) 3.8 GHz.

modes [29]–[32]. As shown in Fig. 11, the SSRR consists of one two-turn SRR and one shorted via connecting the SRR to the metallic ground. The realized gain of the stacked antenna with and without four shorted vias at the boresight direction is shown in Fig. 12. It can be seen that the SSRRs can introduce two radiation nulls (3.55 and 3.8 GHz) in the lower stop band with a quasi-elliptic filtering response. In order to demonstrate the odd and even modes of the SSRR, the current distributions for the stacked antenna with four SSRRs on the middle metallic layer at 3.55 GHz and 3.8 GHz are presented in Fig.13. At 3.55 GHz, the currents on four SSRRs are symmetrical about the shorted vias, which is the even mode of SSRR. At 3.8 GHz, the currents on four SSRRs are odd symmetrical about the shorted vias, which is the odd mode of SSRR. It can be seen that the currents of the antenna are mostly distributed on the SSRRs and edges around SSRRs, and the energy would be dissipated with the oscillation inside the SSRRs.

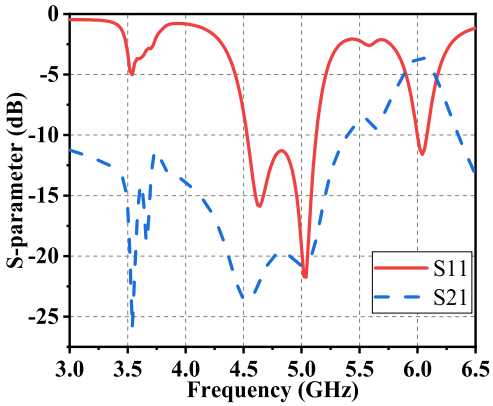

FIGURE 14. Simulated S-parameters of the proposed antenna.

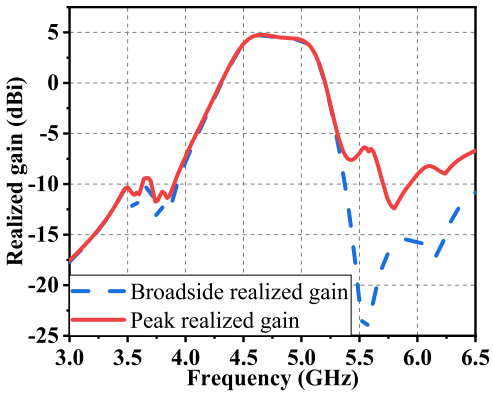

FIGURE 15. Broadside realized gain and peak realized gain of the proposed antenna.

The simulated S-parameters of the proposed antenna are depicted in Fig. 14. As shown in Fig. 14, there are resonances at the frequencies of the radiation nulls introduced by SRRs and SSRRs. As analyzed above, the energy is dissipated inside the SRRs and SSRRs. The broadside realized gain and peak realized gain of the proposed antenna are plotted in Fig. 15. The SRRs and SSRRs can reduce the realized gain in all directions, while the stacked patch introduces radiation null in the broadside direction at the upper frequency band.

C. EFFICIENCY ANALYSIS OF ANTENNA

The aforementioned analyses are based on the antenna printed on two FR4 substrates. In order to better demonstrate the mechanism of the proposed antenna, three antennas using different substrates are simulated, as shown in Fig. 16. The antenna (Ant. 1) in Fig. 16(a) utilizes only one kind of substrate, FR4. The antenna (Ant. 2) in Fig. 16(b) uses the Rogers TMM4 as the substrate, having the permittivity of $\varepsilon_r = 4.4$. The antenna (Ant. 3) in Fig. 16(c) is printed on two kind of substrates, FR4 and Rogers TMM4. The SRRs and SSRRs are printed on FR4, and the patch antenna is printed on Rogers TMM4. The realized gain and radiation efficiency of three antennas are displayed in Fig. 17(a) and (b), respectively. Ant. 1 can achieve radiation nulls, but the efficiency is relatively low due to the high dielectric loss tangent of FR4. Although Ant. 2 uses the substrate with low dielectric loss

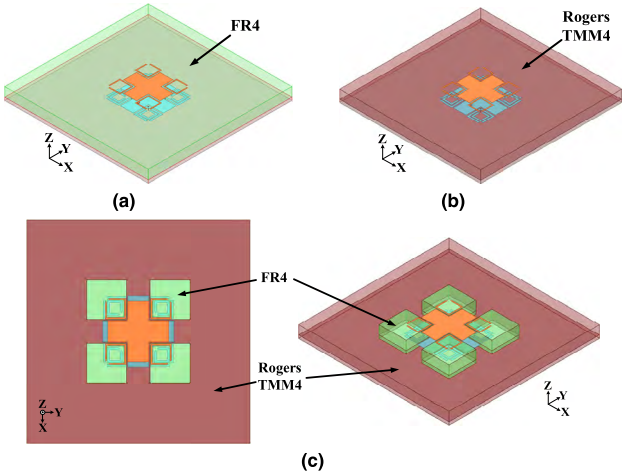

FIGURE 16. Three antennas using different substrates. (a) Antenna using FR4. (b) Antenna using Rogers TMM4. (c) Antenna using FR4 and Rogers TMM4.

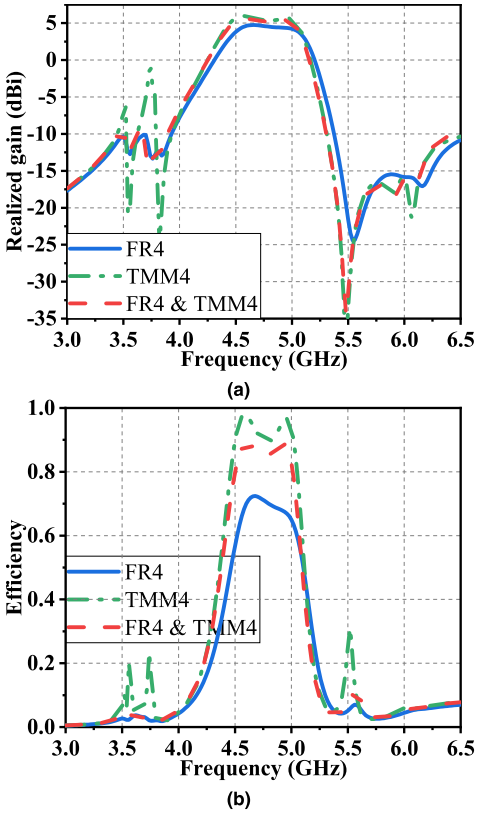

FIGURE 17. (a) Broadside realized gain, and (b) efficiency of three antennas.

tangent, the energy inside the SRRs cannot be dissipated well enough to realize radiation nulls. It can be seen that Ant 3 utilizing two kinds of substrates has high radiation efficiency and can realize radiation nulls at the same time. Just like the previous analysis, the energy would be constrained with the oscillation inside the ring resonators. Therefore, the radiation can be achieved by printing the SRRs and SSRRs on FR4 with high dielectric loss tangent, and the radiation gain and efficiency can be improved by choosing the substrate with low dielectric loss tangent.

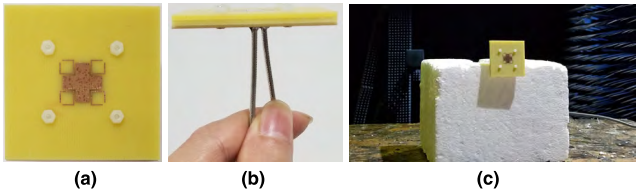

FIGURE 18. The fabrication of the proposed filtering antenna. (a) Top view. (b) Side view. (c) Measurement in the anechoic chamber.

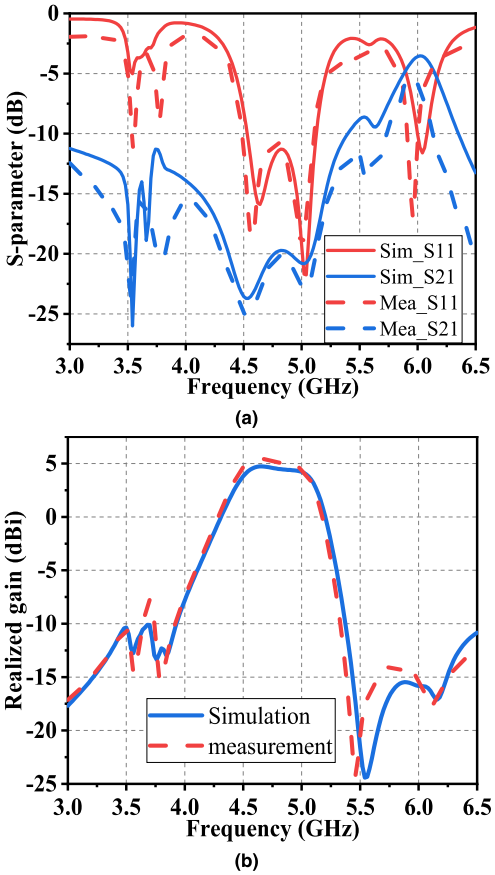

FIGURE 19. Simulated and measured (a) S-parameters, and (b) realized gain.

III. PERFORMANCE OF ANTENNA

A. CASE 1: ANTENNA WITH FR4 SUBSTRATE

For ease of fabrication and integration, the proposed antenna is firstly fabricated on one kind of substrate, FR4, as shown in Fig. 18. The simulation analyses are performed by Ansys HFSS, and the measurements are implemented by the Agilent network analyzer (Agilent N5230A) and far-field measurement system (NSI 2000).

The simulated and measured S-parameters and realized gain are displayed in Fig 19(a) and (b), respectively. As shown in Fig. 19 (a), the measured bandwidth is 4.5-5.1 GHz for S11 < -10 dB, and the measured isolation is better than 22 dB. Fig. 19(b) shows that the average gain is 5 dBi within the whole working band, and four radiation nulls are located at 3.45, 3.75, 5.6 and 6.1 GHz. When the port 1 is excited, the simulated and measured radiation patterns at 4.6, 4.9 and 5.1 GHz in the YOZ and in the XOZ plane are shown

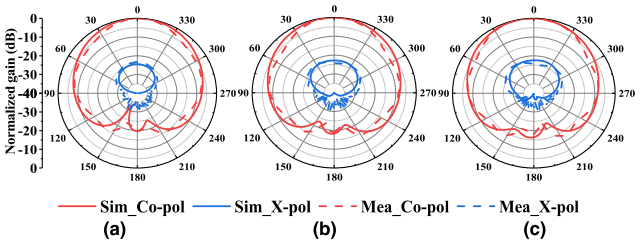

FIGURE 20. Radiation patterns in the YOZ plane at (a) 4.6, (b) 4.9, and (c) 5.1 GHz.

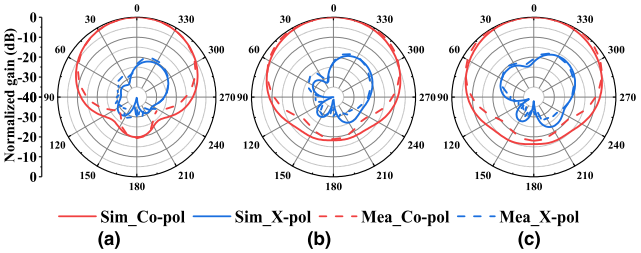

FIGURE 21. Radiation patterns in the XOZ plane at (a) 4.6, (b) 4.9, and (c) 5.1 GHz.

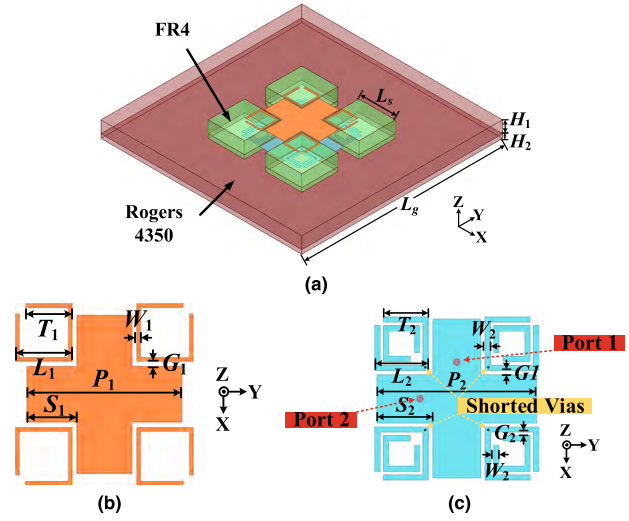

FIGURE 22. The proposed antenna fabricated on two kinds of substrates. (a) Perspective view of the proposed antenna. (b) Top metallic layer. (c) Middle metallic layer. (L_g = 50, L_s = 9, H_1 = 3, H_2 = 1, P_1 = 13.6, P_2 = 16, S_1 = 4.4, S_2 = 5.6, L_1 = 4.6, L_2 = 5, T_1 = 3.8, T_2 = 4.2, G_1 = 0.4, G_2 = 0.3, W_1 = 0.3 and W_2 = 0.5 mm).

in Fig. 20 and Fig. 21, respectively. The radiation patterns are stable and the cross-polarization is lower than −23 dB within the working band. The deviation between the simulated and measured results is attributed to the tolerances of fabrication and measurement.

B. CASE 2: ANTENNA WITH FR4 & ROGERS-4350 SUBSTRATES

In order to improve the efficiency and realized gain, the proposed antenna is simulated and fabricated on two kinds of substrates, FR4 and Rogers-4350, as displayed in Fig. 22 and Fig. 23, respectively. With smaller dielectric loss tangent, the proposed antenna can achieve higher efficiency. With lower dielectric permittivity for the driven patch and the stacked

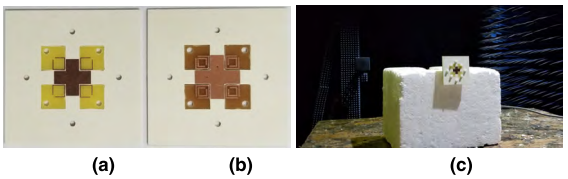

FIGURE 23. The fabrication of the proposed filtering antenna. (a) Top metallic layer. (b) Middle metallic layer. (c) Measurement in the anechoic chamber.

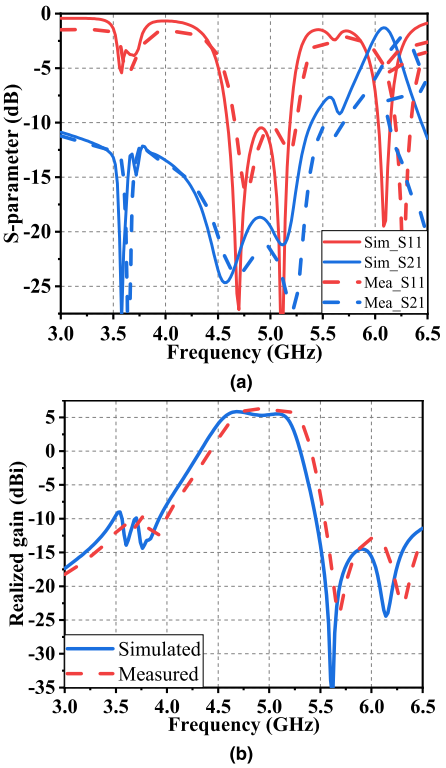

FIGURE 24. Simulated and measured (a) S-parameters, and (b) realized gain.

patch, the proposed antenna would have bigger radiation aperture and achieve higher realized gain. It is worth noting that the geometry of the SRRs is not changed, since the substrate for SRRs does not change, compared to Case 1.

The simulated and measured S-parameters and realized gain are presented in Fig 24(a) and (b), respectively. As plotted in Fig. 24 (a), the measured bandwidth is 4.7-5.2 GHz for S11 < -10 dB, and the measured isolation is better than 21 dB. Compared with Case 1, although Case 2 has lower profile (3mm), Fig. 24(b) shows that the average gain is improved to 6 dBi within the whole working band. Four radiation nulls are located at 3.64, 3.9, 5.68 and 6.32 GHz. The measured working frequency is a little higher than the simulated one, mainly due to the fabrication tolerances with two kinds of substrates. When the port 1 is excited, the simulated and measured radiation patterns at 4.7, 4.9 and 5.1 GHz in the YOZ and in the XOZ plane are shown in Fig. 25 and Fig. 26, respectively. The radiation patterns are stable and the cross-polarization is lower than −20 dB within the working band. The deviation between the simulated and measured results is attributed to the tolerances of fabrication and measurement.

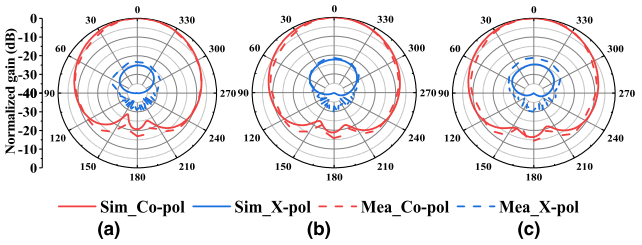

FIGURE 25. Radiation patterns in the YOZ plane at (a) 4.7, (b) 4.9, and (c) 5.1 GHz.

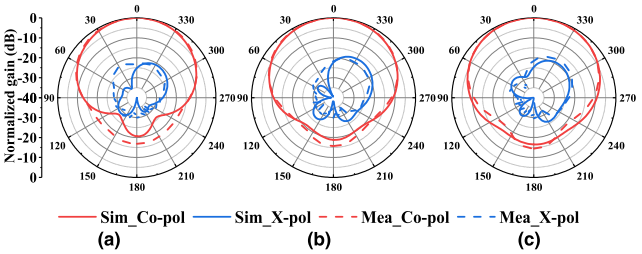

FIGURE 26. Radiation patterns in the XOZ plane at (a) 4.7, (b) 4.9, and (c) 5.1 GHz.

TABLE 1. Comparison of different antennas.

Ref.	Polarization	Cross-Pol (dB)	Gain (dBi)	Extra circuit	Easy for integration
[10]	Single	-22	9.7	No	No
[11]	Single	-20	8.2	No	No
[12]	Single	-23	6.6	No	Yes
[16]	Dual	-20	8	Yes	Yes
[17]	Dual	-23	9.5	Yes	No
[24]	Dual	-29	9.4	No	No
Case 1*	**Dual**	**-22**	**5**	**No**	**Yes**
Case 2#	**Dual**	**-20**	**6**	**No**	**No**

The comparison among the proposed antenna and some reported works is presented in Table 1. Case 1 is the proposed antenna printed on FR4 substrate, and Case 2 is the proposed antenna fabricated on two kinds of substrates, FR4 and Rogers-4350. These reference works are microstrip filtering antennas with unidirectional radiation patterns. The filtering antennas in [10]–[12] can achieve good filtering performance without extra circuit. However, these antennas are all single-polarized and difficult to be extended to dual-polarized ones. Dual-polarized antennas in [16], [17] realize filtering behaviors by cascading extra filtering circuits in the antenna feeding networks. As mentioned above, additional volume and insertion loss of filtering circuits are inescapable. The work [24] utilizes two orthogonal H-shaped feeding lines to ensure a sharp roll-off rate at the lower band edge. The H-shaped feeding network is designed inside the antenna, so the antenna needs to be designed with two substrates and four metallic layers, making the antenna unsuitable for integration. The proposed dual-polarized antenna introduces four radiation nulls at the lower and upper stopbands without extra circuit. Two FR4 substrates of Case 1 are stacked together with three metallic layers, making the antenna suitable for integration. Case 2 can achieve higher realized gain and radiation efficiency with lower dielectric loss tangent and permittivity.

IV. CONCLUSION

A novel dual-polarized filtering patch antenna using SRRs with four radiation nulls is proposed in this paper. Without extra circuit, the proposed antenna achieves radiation nulls by using SRRs and SSRRs. The antenna is fabricated to meet the applications for the 5G band (4.8-5 GHz) for S11 < -10 dB. The antenna implemented on FR4 substrate, which is suitable for integration, can achieves an average gain of 5 dBi, while the antenna fabricated on two substrates, Rogers-4350 and FR4, can improve the realized gain to over 6 dBi.

REFERENCES

[1] X.-Y. Zhang, D. Xue, L.-H. Ye, Y.-M. Pan, and Y. Zhang, "Compact dual-band dual-polarized interleaved two-beam array with stable radiation pattern based on filtering elements," *IEEE Trans. Antennas Propag.*, vol. 65, no. 9, pp. 4566–4575, Sep. 2017.

[2] X. Y. Zhang, Y. Zhang, Y.-M. Pan, and W. Duan, "Low-profile dual-band filtering patch antenna and its application to LTE MIMO system," *IEEE Trans. Antennas Propag.*, vol. 65, no. 1, pp. 103–113, Jan. 2017.

[3] B. Zhang and Q. Xue, "Filtering antenna with high selectivity using multiple coupling paths from source/load to resonators," *IEEE Trans. Antennas Propag.*, vol. 66, no. 8, pp. 4320–4325, Aug. 2018.

[4] Q.-S. Wu, X. Zhang, and L. Zhu, "An improved method for accurate extraction of coupling coefficient between a lossy radiator and a lossless resonator in filtering antennas," *IEEE Access*, vol. 6, pp. 39927–39935, 2018.

[5] K.-D. Xu, H. Xu, and Y. Liu, "Low-profile filtering end-fire antenna integrated with compact bandstop filtering element for high selectivity," *IEEE Access*, vol. 7, pp. 8398–8403, 2019.

[6] L.-H. Wen, S. Gao, Q. Luo, Z. Tang, W. Hu, Y. Yin, Y. Geng, and Z. Cheng, "A balanced feed filtering antenna with novel coupling structure for low-sidelobe radar applications," *IEEE Access*, vol. 6, pp. 77169–77178, 2018.

[7] J.-F. Qian, F.-C. Chen, and Q.-X. Chu, "A novel Tri-band patch antenna with broadside radiation and its application to filtering antenna," *IEEE Trans. Antennas Propag.*, vol. 66, no. 10, pp. 5580–5585, Oct. 2018.

[8] J.-F. Qian, F.-C. Chen, Y.-H. Ding, H.-T. Hu, and Q.-X. Chu, "A wide stopband filtering patch antenna and its application in MIMO system," *IEEE Trans. Antennas Propag.*, vol. 67, no. 1, pp. 654–658, Jan. 2019.

[9] K. Xu, J. Shi, X. Qing, and Z. N. Chen, "A substrate integrated cavity backed filtering slot antenna stacked with a patch for frequency selectivity enhancement," *IEEE Antennas Wireless Propag. Lett.*, vol. 17, no. 10, pp. 1910–1914, Oct. 2018.

[10] X. Y. Zhang, W. Duan, and Y.-M. Pan, "High-gain filtering patch antenna without extra circuit," *IEEE Trans. Antennas Propag.*, vol. 63, no. 12, pp. 5883–5888, Dec. 2015.

[11] P. F. Hu, Y. M. Pan, X. Y. Zhang, and B.-J. Hu, "A filtering patch antenna with reconfigurable frequency and bandwidth using F-shaped probe," *IEEE Trans. Antennas Propag.*, vol. 67, no. 1, pp. 121–130, Jan. 2019.

[12] J. Y. Jin, S. Liao, and Q. Xue, "Design of filtering-radiating patch antennas with tunable radiation nulls for high selectivity," *IEEE Trans. Antennas Propag.*, vol. 66, no. 4, pp. 2125–2130, Apr. 2018.

[13] C. Meng, J. Shi, and J.-X. Chen, "Flat-gain dual-patch antenna with multi-radiation nulls and low cross-polarisation," *Electron. Lett.*, vol. 54, no. 3, pp. 114–116, Feb. 2018.

[14] Y. M. Pan, P. F. Hu, X. Y. Zhang, and S. Y. Zheng, "A low-profile high-gain and wideband filtering antenna with metasurface," *IEEE Trans. Antennas Propag.*, vol. 64, no. 5, pp. 2010–2016, May 2016.

[15] W. Yang, S. Chen, Q. Xue, W. Che, G. Shen, and W. Feng, "Novel filtering method based on metasurface antenna and its application for wideband high-gain filtering antenna with low profile," *IEEE Trans. Antennas Propag.*, vol. 67, no. 3, pp. 1535–1544, Mar. 2019.

[16] C.-X. Mao, S. Gao, Y. Wang, F. Qin, and Q.-X. Chu, "Multimode resonator-fed dual-polarized antenna array with enhanced bandwidth and selectivity," *IEEE Trans. Antennas Propag.*, vol. 63, no. 12, pp. 5492–5499, Dec. 2015.

[17] C.-X. Mao, S. Gao, Y. Wang, Q. Luo, and Q.-X. Chu, "A shared-aperture dual-band dual-polarized filtering-antenna-array with improved frequency response," *IEEE Trans. Antennas Propag.*, vol. 65, no. 4, pp. 1836–1844, Apr. 2017.

[18] C.-X. Mao, S. Gao, Y. Wang, Y. Liu, X.-X. Yang, Z.-Q. Cheng, and Y.-L. Geng, "Integrated dual-band filtering/duplexing antennas," *IEEE Access*, vol. 6, pp. 8403–8411, 2018.
[19] H. Huang, Y. Liu, and S. Gong, "A broadband dual-polarized base station antenna with anti-interference capability," *IEEE Antennas Propag. Lett.*, vol. 16, pp. 613–616, 2016.
[20] Y. M. Pan, P. F. Hu, K. W. Leung, and X. Y. Zhang, "Compact single-/dual-polarized filtering dielectric resonator antennas," *IEEE Trans. Antennas Propag.*, vol. 66, no. 9, pp. 4474–4484, Sep. 2018. doi: 10.1109/TAP.2018.2845457.
[21] H. Tang, C. Tong, and J.-X. Chen, "Differential dual-polarized filtering dielectric resonator antenna," *IEEE Trans. Antennas Propag.*, vol. 66, no. 8, pp. 4298–4302, Aug. 2018.
[22] C.-M. Meng, J. Wang, and J. Shi, "A substrate integrated cavity-fed dual-polarized filtering patch antenna with high isolation," *Int. J. RF Microw. Comput. Aided Eng.*, vol. 29, no. 9, Sep. 2019.
[23] H. Chu and Y.-X. Guo, "A filtering dual-polarized antenna subarray targeting for base stations in millimeter-wave 5G wireless communications," *IEEE Trans. Compon., Packag., Manuf. Technol.*, vol. 7, no. 6, pp. 964–973, Jun. 2017.
[24] W. Duan, X. Y. Zhang, Y.-M. Pan, J.-X. Xu, and Q. Xue, "Dual-polarized filtering antenna with high selectivity and low cross polarization," *IEEE Trans. Antennas Propag.*, vol. 64, no. 10, pp. 4188–4196, Oct. 2016.
[25] Q.-S. Wu, X. Zhang, and L. Zhu, "Co-design of a wideband circularly polarized filtering patch antenna with three minima in axial ratio response," *IEEE Trans. Antennas Propag.*, vol. 66, no. 10, pp. 5022–5030, Oct. 2018.
[26] A. K. Sahoo, R. D. Gupta, and M. S. Parihar, "Circularly polarised filtering dielectric resonator antenna for X-band applications," *IET Microw., Antennas Propag.*, vol. 12, no. 9, pp. 1514–1518, Jul. 2018.
[27] J. Y. Siddiqui, C. Saha, and Y. M. M. Antar, "Compact SRR loaded UWB circular monopole antenna with frequency notch characteristics," *IEEE Trans. Antennas Propag.*, vol. 62, no. 8, pp. 4015–4020, Aug. 2014.
[28] M. Barbuto, F. Trotta, F. Bilotti, and A. Toscano, "Horn antennas with integrated notch filters," *IEEE Trans. Antennas Propag.*, vol. 63, no. 2, pp. 781–785, Feb. 2015.
[29] W. Jiang, W. Shen, T. Wang, Y. M. Huang, Y. Peng, and G. Wang, "Compact dual-band filter using open/short stub loaded stepped impedance resonators (OSLSIRs/SSLSIRs)," *IEEE Microw. Wireless Compon. Lett.*, vol. 26, no. 9, pp. 672–674, Sep. 2016.
[30] D. Li, Y. Zhang, K. Song, K. Xu, and J. L.-W. Li, "Miniaturized close dual-band bandpass filter based on short stub-loaded stepped-impedance resonators," *Electromagnetic*, vol. 35, no. 1, pp. 49–58, 2015.
[31] Y. Guo, X. Tang, K. D. Xu, and J. Ai, "Dual high-selectivity band-notched UWB monopole antenna using simple dual-mode resonator and high-impedance lines," *Int. J. Microw. Wireless Technol.*, vol. 9, no. 4, pp. 923–926, May 2016.
[32] Y. J. Guo, K. D. Xu, and X. H. Tang, "Multi-functional ultra-wideband monopole antenna with high frequency selectivity," *Appl. Comput. Electromagn. Soc. J.*, vol. 33, no. 1, pp. 37–42, Jan. 2018.

YAOHUI ZHANG received the B.S. degree in electromagnetic wave propagation and antenna, from the University of Electronic Science and Technology of China (UESTC), Chengdu, China, in 2014, where he is currently pursuing the Ph.D. degree in electromagnetic field and microwave technology. His research interests include compact and wideband antennas and microwave filter.

YONGHONG ZHANG received the B.S., M.S., and Ph.D. degrees from the University of Electronic Science and Technology of China (UESTC), Chengdu, China, in 1992, 1995, and 2001, respectively. He is currently a Full Professor with the School of Electronic Science and Engineering, UESTC. From 1995 to 2002, he was a Lecturer with the UESTC. From 2002 to 2004, he was a Postdoctoral Fellow with the Department of Electronic Engineering, Tsinghua University, Beijing, China. Since 2004, he has been with UESTC. He is a Senior Member of the Chinese Institute of Electronics. His research interests include microwave and millimeter wave technology and applications.

DAOTONG LI (S'15–M'16) received the Ph.D. degree in electromagnetic field and microwave technology from the University of Electronic Science and Technology of China (UESTC), Chengdu, China, in 2016.

He is currently with the Center of Aircraft TT&C and Communication, Chongqing University, Chongqing. Since 2015, he has been a Visiting Researcher with the Department of Electrical and Computer Engineering, University of Illinois at Urbana—Champaign, Urbana, IL, USA, with financial support from the China Scholarship Council. He has authored or coauthored over 50 peer-reviewed journal or conference papers. Since 2014, he has been a reviewer for some international journals. His current research interests include RF, microwave and millimeter-wave technology and applications, antennas, devices, circuits and systems, and passive and active (sub-) millimeter-wave imaging and radiometer.

Dr. Li was a recipient of the Outstanding Graduate Awards from the Sichuan province and UESTC, in 2016, the National Graduate Student Scholarship from the Ministry of Education, China, and Tang Lixin Scholarship. He is serving as a Reviewer for several IEEE and IET journals, and many international conferences as a TPC Member, a Session Organizer, and the Session Chair.

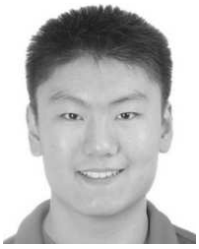

ZHONGQIAN NIU was born in Luoyang, Henan, China, in 1991. He received the B.E. degree in electronic science and technology from the University of Electronic Science and Technology of China (UESTC), Chengdu, China, in 2014, where he is currently pursuing the Ph.D. degree in terahertz solid-state devices and systems with the School of Electronic Science and Engineering. His research interests include terahertz high speed communication system, terahertz mixers, and other terahertz devices.

YONG FAN (M'05) received the B.E. degree from the Nanjing University of Science and Technology, Jiangsu, China, in 1985, and the M.S. degree from the University of Electronic Science and Technology of China (UESTC), Chengdu, China, in 1992. He is currently a Full Professor with the School of Electronic Science and Engineering, University of Electronic Science and Technology of China. He has authored or coauthored more than 200 papers. His current research interests include electromagnetic theory, millimeter-wave and terahertz circuits, and communication technology. He is a Senior Member of the Chinese Institute of Electronics.